A Mathematical Expression to Determine Copper Losses in Switching-Mode Power Supplies Transformers Including Geometry and Frequency Effects

Juan Manuel Lopera, *Member, IEEE*, Miguel Jose Prieto, *Member, IEEE*, Juan Díaz, *Member, IEEE*, and Jorge García, *Senior Member, IEEE*

***Abstract*—High-frequency copper losses, or copper losses produced during switching in switching-mode power supplies, are very much related to variations of the magnetic field distribution within the core window. When operating at high frequency, the current flowing through the windings of a magnetic component experiences redistribution across the section of the conductor due to skin and proximity effects. Current redistribution depends not only on actual frequency, but also on conductor size and layer distribution. While previous works aim to optimize windings size by considering just the current flowing through that winding, this paper shows that, in most of the cases, current redistribution is strongly affected by the currents at the other transformer windings, which should also be taken into account. This paper derives a mathematical expression to calculate the evolution, in the time domain, of the magnetic field during the switching, which will be later used to obtain the current density distribution and copper losses in the component. An easy-to-calculate expression will be derived that allows magnetic windings to be analyzed and/or optimized, because losses are expressed as a function of the winding geometry and position. An application example is also included. All the equations derived are verified by comparing them with the results obtained from a differential equations solver, and with previous works when applicable. Experimental results are also provided.**

***Index Terms*—High-frequency copper losses, switching-mode power supplies (SMPS), transformers.**

I. Introduction

REQUIREMENTS set on switching-mode power supplies (SMPS) continue to become more demanding in terms of size, weight, efficiency, electromagnetic compatibility, time to market, etc. In this regard, magnetic components play an important role in the design of SMPS, since they are the bulkiest components in the supply (30–50% of the converter volume is engaged by inductors and/or transformers), they are an important source of radiation, they must be designed for each specific application and they significantly contribute to reducing overall efficiency due to their core and copper losses.

Manuscript received February 7, 2014; revised April 1, 2014; accepted March 12, 2014. Date of publication May 16, 2014; date of current version November 3, 2014. Recommended for publication by Associate Editor T. M. Lebey.

The authors are with the Electronic Technology Department, Universidad de Oviedo, 33203 Gijón, Spain (e-mail: lopera@uniovi.es; mike@uniovi.es; jdiazg@uniovi.es; garciajorge@uniovi.es).

Digital Object Identifier 10.1109/TPEL.2014.2324977

Copper losses in SMPS are not easy to quantify, for they are seriously affected by the high frequency this type of converters use. When operating at high frequency, the current flowing through the windings of a magnetic component experiences redistribution across the section of the conductor due to skin and proximity effects. This results in a reduction of the effective section the current flows through and, hence, in higher power loss. To this respect, it must be noted that one of the main difficulties designers have to deal with is determining what "high frequency" means for their magnetic components. The aforementioned current redistribution depends not only on actual frequency, but also on conductor size and layer distribution (i.e., primary/secondary interleaving). Thus, it is possible that a 10-kHz design using 3-mm wires suffers more severe "high-frequency effects" than a 100-kHz design using 0.1-mm wires.

It can, therefore, be understood that conductor size or winding strategy can dramatically influence the behavior of this kind of components, which in turn explains the need to have them specifically designed for each application.

Although the most appropriate method to study the influence of the skin and proximity effects is by means of finite-element analysis (FEA) [1], [2], this is hardly ever done unless the goal is optimizing an already existing design. In most of the cases, designers lack the expertize or the time (or both) to use this kind of FEA tools, but, even if they did not, they would not know the actual currents in the design, for they will depend on the exact magnetic design. Therefore, at least for these early design stages, it is necessary to have an alternative simpler way to estimate the copper losses related to a given design.

Several works have been published that offer a solution to consider these high-frequency effects in windings [3]–[7], but they mostly focus on sinusoidal waveforms, which is seldom the kind of excitation present in SMPS. Other authors [8]–[19] aim to extend this method by considering an approximate current waveforms and performing a harmonic analysis that brings them back to sinusoidal-excitation expressions. Although useful, these works do not allow designers to establish a clear relation between the losses obtained and the relative positions of the several magnetic windings or layers.

The approach followed by these papers consists of taking n consecutive layers of a given winding (winding portions) and analyzing their short-circuit MMF diagram in order to come up with an equation that allows optimum conductor size to be

derived (e.g., [13, Fig. 2]). This equation, expressed in terms of the harmonics of the current flowing through that winding, is said to take into consideration both skin and proximity effects. However, as will be later explained in Section II, this is only true for two-winding side-by-side transformers. The magnetic field distribution in transformers with three or more windings (such as those included in half-bridge or push–pull topologies, for instance) depends not only on the current flowing through a given winding but also on that flowing through other windings (complete proximity effect) and the methods derived in those papers are no longer applicable.

This paper aims to derive a generic mathematical expression that can be used with the waveforms typically found in SMPS to calculate the copper losses in the magnetic components they include. In order to do so, the general differential equation for the variation of the magnetic field will be used, and a so far unexplored approach will be used: directly solving that equation in the time domain instead of doing so in the frequency domain.

As will be shown later, some new concepts will appear due to this approach, such as separating copper losses into two categories: conduction losses and switching losses (as is the cases with semiconductor devices).

Some assumptions are made in order to achieve this goal.

1) *Currents through the windings are considered to be square:* This is not the most usual waveform shape in actual converters, but it will serve the purpose of analyzing switching copper losses. Also, real waveforms will not be known until the final component has been designed and its parasitics can be taken into account by using accurate models and circuit simulators. Such simulations will provide more exact results, but designers will lack information about the relation between copper losses and winding layer dimensions.
2) *One-dimensional fields within the winding area:* The fields within the magnetic component are always considered to be 1-D, with the magnetic field being mainly parallel to the winding layers and varying across the width of the winding area. This is a common assumption made in the literature because in spite of not being valid for all the designs, it is applicable to most magnetic components. This involves that some situations that give rise to 2-D effects (such as the fringing effect close to the gap of flyback transformers [20]) must be avoided.

Using these assumptions, a simplified easy to calculate expression will be derived that allows magnetic windings to be analyzed and/or optimized.

Section II includes a review of high-frequency effects in magnetic components, focusing on the variations experienced by the magnetic field during the switching.

Section III derives a mathematical expression to calculate the evolution of the magnetic field during the switching, which will be later used in Section IV to obtain the current density distribution and copper losses in the component.

Section V includes an application example showing how to determine winding losses by using the method presented in this paper, while Section VI is used to verify the obtained equations by comparing them with the results obtained from a differential equations solver.

Finally, some conclusions are provided.

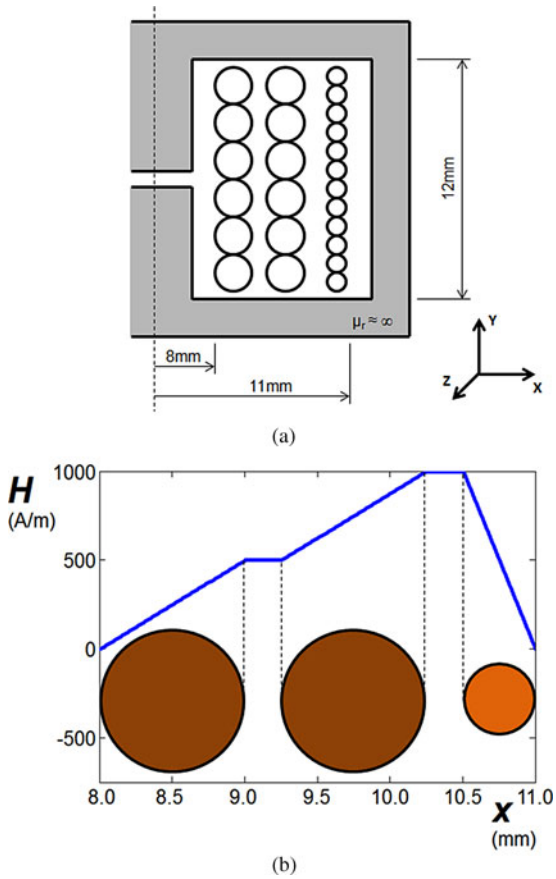

Fig. 1. (a) Transformer considered and (b) corresponding low-frequency MMF diagram in a short-circuit test.

II. High-Frequency Effects

Consider a three-layer transformer as that shown in Fig. 1(a), whose primary winding is composed of 12 turns separated into two layers and whose secondary is the third layer. Conductor diameters are 1 mm for the primary and 0.5 mm for the secondary. Assuming that the magnetic field in the core is negligible (since $\mu_r = \infty$), that fields are 1-D (which is the usual case in most magnetic components), and that current is uniformly distributed (constant current density), the low-frequency MMF diagrams across the core window when a short-circuit test is performed can be calculated using Ampere's law, to be that represented in Fig. 1(b).

It must be noted, though, that by "low-frequency," we actually mean any frequency at which current is distributed uniformly across the conductor area. However, when this is not the case and the transformer experiences high-frequency excitation—or sudden changes, for that matter—redistribution of the magnetic field takes place, and since it cannot easily follow so fast variations, the actual shape of the magnetic field distribution is that shown in Fig. 2. This phenomenon has already been documented

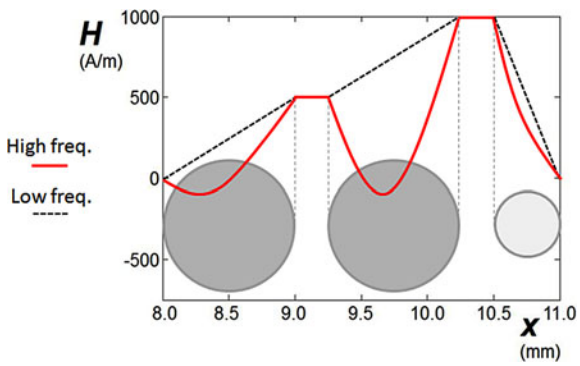

Fig. 2. High-frequency magnetic field distribution in a short-circuit test.

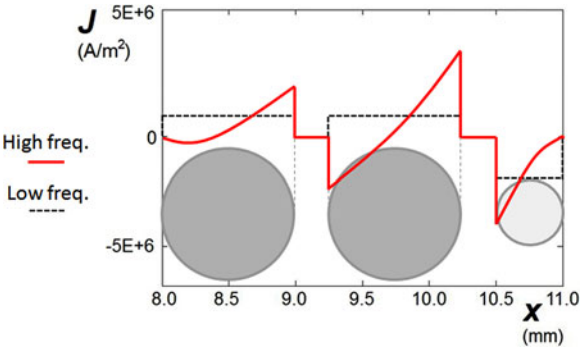

Fig. 3. High-frequency current density in a short-circuit test.

by various authors (such as [21]), all of them considering sinusoidal excitation.

If the sinusoidal-state constraint must be eliminated, Maxwell equations must be used

$$\nabla \times \vec{H} = \vec{J} + \frac{\partial \vec{D}}{\partial t}, \quad \nabla \cdot \vec{D} = \rho$$

$$\nabla \times \vec{E} = -\frac{\partial \vec{B}}{\partial t}, \quad \nabla \cdot \vec{B} = 0. \tag{1}$$

By neglecting displacement currents in the first of these equations, it can be rewritten for 1-D fields as follows:

$$\frac{\partial H}{\partial x} = J. \tag{2}$$

Hence, high-frequency current density can also be derived. Fig. 3 is a good example of what skin and proximity effects can lead to. It can be observed that this current density is nonuniform, which largely increases copper losses.

Note that the current densities inside the two layers of the same size are very different from one another. While in the inner one the current is concentrated near the surface at the right, in the central layer a negative current density (which also produces copper losses) is induced at the left, whereas a large current density appears at the right in order to maintain the total conductor current. The central layer losses (J-squared) might easily be tens of times higher than those in the inner layer; this can be rather surprising for a nonexpert designer because actually the conductors in both layers are equal.

All this lets us conclude that high-frequency copper losses, or copper losses produced during switching in SMPS, are very much related to variations of the magnetic field distribution within the core window. Thus, in order to derive current density in the windings (and hence, copper losses), the actual evolution of the magnetic field must be first obtained. This will be done by considering Maxwell equations provided in (1), and the following relations that apply to the materials typically used in magnetic component windings:

$$\vec{B} = \mu \cdot \vec{H}, \quad \vec{D} = \varepsilon \cdot \vec{E}$$

$$\vec{J} = \sigma \cdot \vec{E}, \quad \rho = 0. \tag{3}$$

Also, assuming 1-D fields, as previously indicated, and considering the axes represented in Fig. 1

1) magnetic field, *H*, follows the direction of the *Y*-axis and its value changes along the *X*-axis: $H = H_y(x)$;
2) electric field, *E*, and current density, *J*, follow the direction of the *Z*-axis and their values change along the *X*-axis: $E = E_z(x)$ and $J = J_z(x)$.

Taking all this into account, and considering that the magnetic field also changes with time, the following expression can be obtained:

$$\frac{\partial^2 H_y(x,t)}{\partial x^2} = \mu \cdot \sigma \cdot \frac{\partial H_y(x,t)}{\partial t} + \mu \cdot \varepsilon \cdot \frac{\partial^2 H_y(x,t)}{\partial t^2}. \tag{4}$$

Neglecting displacement currents (represented by the second term in the equation), the resulting expression is simply

$$\frac{\partial^2 H_y(x,t)}{\partial x^2} = \mu \cdot \sigma \cdot \frac{\partial H_y(x,t)}{\partial t}. \tag{5}$$

This is the equation that must be solved in order to derive the evolution of the magnetic field within the core window and, hence, the current redistribution inside the windings that results in the so-called skin or proximity effects.

In fact, these effects are the key point when designing high-frequency transformers. When copper losses are to be reduced, the first impulse is always increasing the conductor section, thus reducing dc resistance and, consequently, losses. Unfortunately, this basic idea does not work so well in high-frequency transformers because of the current induced due to the proximity effect.

When the conductor section is increased, a lower dc resistance will be actually measured and the dc part of the copper losses will decrease. However, copper losses produced when usual SMPS-operating points are considered may become larger when using thicker conductors. The use of wider conductors may result in more layers being needed, which will in turn give rise to larger induced currents, i.e., higher copper losses.

This topic is not new, and there have been lots of papers dealing with it during the last 50 years. An interesting guide to several significant articles about these effects can be found in [3]. Nevertheless, we will highlight some of them here, to clearly see the differences of the method presented in this paper with that introduced by previous works.

Dowell [4] studied the effects of eddy currents, considering sinusoidal currents in transformer windings and derived a method for calculating the variation of winding resistance and leakage

inductance as a function of frequency for single-layer transformers, multilayer transformers, and transformer with sectionalized windings. The method consists in dividing the winding into portions, calculating the dc resistance and dc leakage inductance of each of these portions, and then multiplying these dc values by appropriate factors to obtain the corresponding ac values.

Perry [5] reexamined the classical 1-D magnetic field and eddy current distribution (also for dc currents) considering a number of consecutive layers both with equal thickness for all layers and with specific layer thickness. For the second case, he showed that the conductor thickness which results in minimum dissipation depends on the relative position of the layer.

Ferreira [18] considered ac waveforms as well, and presented a method to calculate the ac resistance of round conductor windings which yields more accurate results than the previous 1-D methods, which considered rectangular conductors.

Nan and Sullivan [19] studied the different results of Dowell and Ferreira methods, by using finite-elements method (note that none of previous mentioned works offered any experimental result) and introduced a new formula, based on modifying the Dowell method.

Designers may use any of these methods to select the theoretical conductor size that best satisfies their requirements, and then use an impedance analyzer in order to verify whether the ac resistance thus obtained is low enough for their application.

However, most SMPS do not operate in sinusoidal regime. Instead, the voltages and currents involved are mostly square, which gives rise to switching losses not reflected by the sinusoidal approach. This is solved in [8], [9], and [22] by employing Fourier analysis techniques, although other possibility is defined in [11] based on the definition of an effective frequency that accounts for the high-frequency content of the actual waveform.

Unfortunately, simple graphs that allow designers to derive optimum winding size by simply considering the number of consecutive layers and the skin depth (like the ones provided in some of the works mentioned above) do not take into account actual harmonic content in the waveforms. Thus, if we decide to optimize winding size for the main harmonic, very poor results might be obtained associated with the dc component or due to higher harmonic losses contribution.

Trying to simplify the design process, Hurtey *et al.* [13] presented a new formula to derive optimum foil or layer thickness, without the need for Fourier coefficients or calculations at harmonic frequencies. The formula requires only the RMS value of the current waveform and the RMS value of its derivative. Although they offer simple expressions for the most common waveforms in SMPS, all of these expressions need current rise and fall times to be known, which is something difficult to accurately specify beforehand.

Whatever the approach, all these works, whether they include harmonic analysis or not, derive their expression considering that the magnetic field of the windings depends only on the winding current itself. Thus, it is possible to establish a relationship between the induced losses (magnetic field changes dependent) and the dc losses (current dependant). That will be true for innermost and outermost windings in a transformer (just using Ampere's law), but it is not true for the intermediate windings (or layers, if interleaving is applied). Thus, they only consider a phenomenon that might be referred to as the "self-proximity" effect.

Even for transformers with only two windings, in which winding magnetic field only depends on winding current (and maybe a dc magnetizing field, e.g., flyback topology), the ac approach used in the above-mentioned methods might not be appropriate. Such an ac approach considers that, in a converter period, the magnetic field varies from 0 to its maximum value, then returns to 0, goes all the way down to the negative peak value, and finally, returns to 0. However, in one converter period of most of actual SMPS, magnetic field just varies between 0 and its maximum value.

In converters including transformers with more than two windings, several changes in the magnetic field may occur, as illustrated in the following example.

Fig. 4(a) and (b) shows a half-bridge converter and the ideal current waveforms flowing through the transformer windings, respectively. We will assume that all the three windings are made up of two layers each, and arranged from the inside to the outside of the core as follows: first winding A, then winding B, and finally the primary winding [see Fig. 4(c)]. It is possible to derive the magnetic field in the two layers of winding A (the innermost winding in the transformer) by simply applying Ampere's law considering the current flowing through that winding. Similarly, the magnetic field in all the layers of the primary winding (the outmost winding in the transformer) can also be calculated as a function of the primary current only. However, the magnetic field at a given point in the layers of winding B is a function of current i_B and of the other currents in the transformer. This can be easily seen by comparing Fig. 4(b) and (d); the waveforms for current i_A and magnetic field H_{a1}, which correspond to the innermost winding, are identical, whereas those for current i_B and magnetic field H_{b1} are not. Therefore, the aforementioned works, which derive copper losses taking into account only the current flowing through a given winding, cannot be used to determine losses in the central winding of the transformer considered in the example.

This effect would be much more obvious if interleaving techniques are used. In this case, this influence (complete proximity effect) appears in all the layers, excepting the innermost and the outmost ones. That is, the evolution of the magnetic field at both sides of each layer will depend on several currents.

These proximity influence is present in all three-winding transformers (such as those in half-bridge, push–pull, full-bridge, etc.) and also in two-winding transformers when interleaving is used (which is usually the best option for minimizing high-frequency copper losses).

Vandelac and Ziogas [22] already explained this in 1988: a magnetic field harmonic analysis (instead of a current harmonic analysis) must be done in order to solve the field differential equation by using the $j{\cdot}\omega$ term. Since such a magnetic field harmonic analysis is to be performed for all the points in the core window, and the harmonics are different for each of the layers a given winding, analyzing magnetic structures by means of this method is complex and laborious.

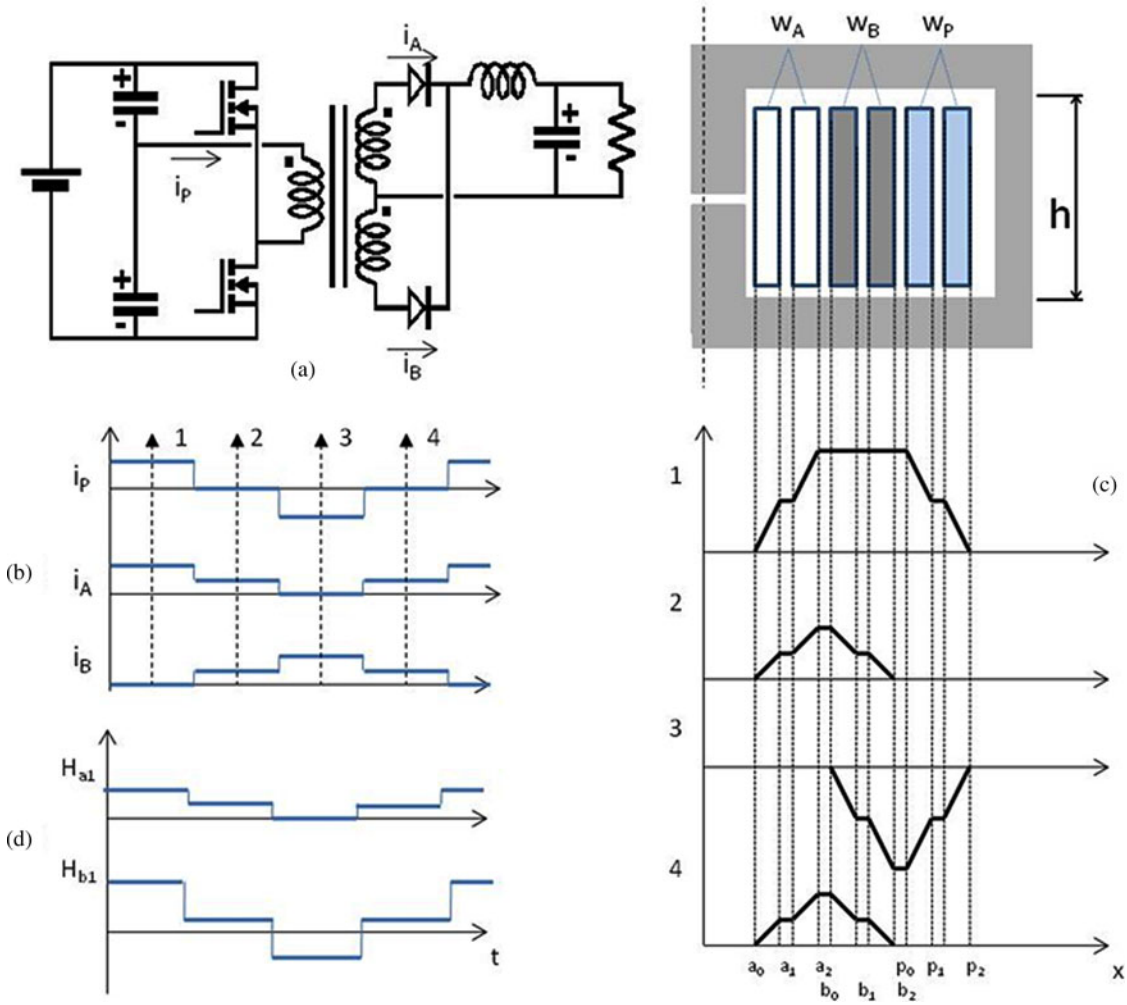

Fig. 4. Half-bridge converter: (a) Schematic, (b) currents, (c) MMF at the four instants indicated, and (d) magnetic fields versus time at two different winding points.

Even though the topic dealt with in this paper can be considered to be rather old (note that the first of the referenced works dates back to 1966), the authors consider that a simple accurate method for optimum high-frequency transformer design has not been developed yet.

In this paper, a time-domain solution is investigated, aiming to obtain a generic solution that can be directly used for the situations typically dealt with in SMPS. This time-domain approach, so far unexplored, will result in an expression consisting of two clearly differentiated parts: a dc term that decreases as conductor size is increased, and a switching loss term that gets higher as conductors are made larger; also, the switching loss term depends on the winding distribution and will be larger for layers placed in a position where magnetic field variations are larger.

III. Proposed Method

As far as high-frequency copper loss is concerned, the most critical situation is that in which current through the winding experiences rapid variations. This might be the result of the commutation of the current by switches or the steering of the current from one winding to another, as in push–pull transformers or flyback transformers.

The analysis that follows will be applied on a foil winding of the magnetic component. When required, layers of round-wire conductors must be transformed into their equivalent foil conductor as described in [4] and later used by other authors [8], [10]–[12], [21], [22]. Fig. 5 summarizes the steps required for such transformation, which involves the use of a "layer porosity" factor in order to compensate for the increased cross-sectional area of the foil layer produced by the stretching. This factor will be considered throughout this paper by including an equivalent conductivity, σ', in all the expressions related to the equivalent one-turn foil layer through which a current $N{\cdot}i$ flows. The value of such equivalent conductivity can be obtained as follows:

$$\sigma' = \frac{N \cdot d \cdot \sqrt{\pi}}{2 \cdot b_w} \cdot \sigma = \eta \cdot \sigma \tag{6}$$

where N is the number of turns in the original layer, d is the diameter of each of those turns, and b_w is the breadth of the core window; η is the layer porosity factor. Obviously, this equivalent

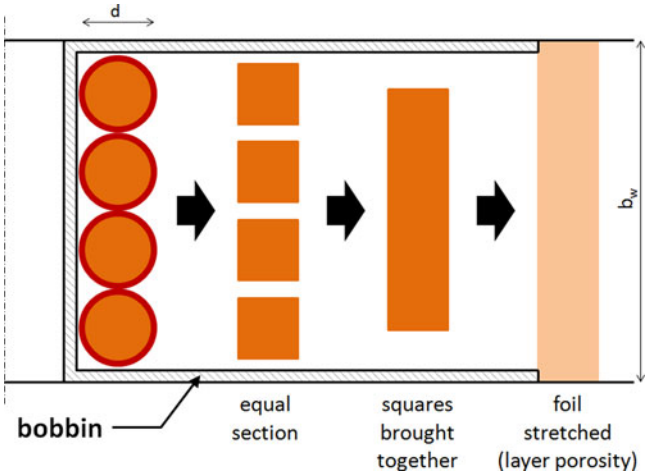

Fig. 5. Transformation of a round-wire layer into a foil layer.

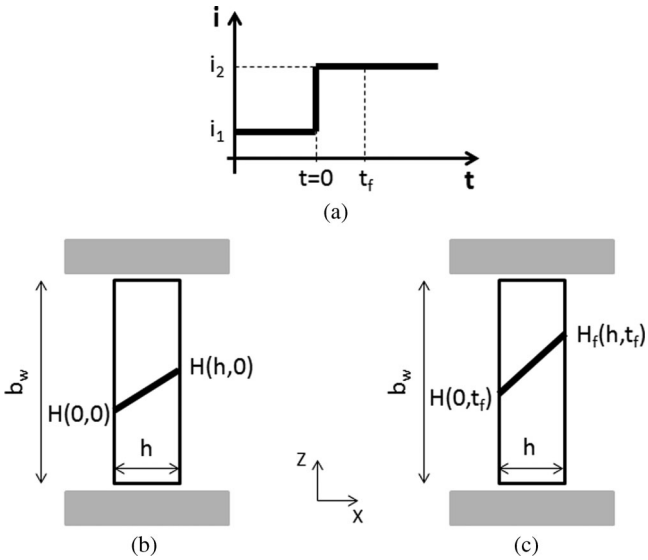

Fig. 6. (a) Current variation in a winding and steady-state magnetic field distributions resulting (b) before and (c) after the change.

foil conversion will produce some errors [18], [19], especially for very low porosity factors. Nevertheless, this approach has been used by all the papers trying to obtain high-frequency losses expressions, since a 2-D approach would only be feasible when using finite-element modeling.

Consider the case depicted in Fig. 6(a) in which the current through an *N*-turn winding suddenly changes from value i_1 to value i_2. This is not the most typical case in SMPS, where either transformer windings hold some current or they have no current at all ($i_1 = 0$ or $i_2 = 0$). However, this more general approach will still be considered so as to make the method proposed have an application range as broad as possible.

This sudden variation must be dealt with by the copper in the winding and results in a current redistribution that will not take place instantaneously. For the moment, let us assume that the new current density has reached its final uniform value after a given time t_f—we will come back to this later on. Fig. 6(b)

$$\frac{\partial^2 H(x,t)}{\partial x^2} = \mu \cdot \sigma' \cdot \frac{\partial H(x,t)}{\partial t}$$

t=0 (initial situation): $H(x,0) = H(0,0) + \dfrac{H(h,0) - H(0,0)}{h} \cdot x$

$t=t_f$ (final situation): $H(x,t_f) = H(0,t_f) + \dfrac{H(h,t_f) - H(0,t_f)}{h} \cdot x$

Boundary conditions: $H(0,t)$ & $H(h,t)$ constant $0 < t \le t_f$

Fig. 7. Equations that allow the magnetic field distribution inside a winding to be obtained.

and (c) shows the magnetic field distribution inside the winding before, $H(x,0)$, and after, $H(x,t_f)$, the change in the current flowing through it. These low-frequency MMF diagrams can be easily obtained and constitute the starting point for the method presented in this paper.

The equations that define the magnetic field distributions are

$$H(x,0) = H(0,0) + \frac{H(h,0) - H(0,0)}{h} \cdot x \quad (7)$$

$$H(x,t_f) = H(0,t_f) + \frac{H(h,t_f) - H(0,t_f)}{h} \cdot x \quad (8)$$

where the values of $H(0,0)$, $H(h,0)$, $H(0,t_f)$, and $H(h,t_f)$ also depend on the other windings in the magnetic component. Two low-frequency MMF diagrams are needed: one for the instant before the switching ($t = 0$), and another one corresponding to the time at which the switching has been completed ($t = t_f$). Note that, as soon as the winding starts conducting the new current i_2, the magnetic field values at its boundaries immediately turn to $H(0,t_f)$ and $H(h,t_f)$, respectively. It is the field evolution within the layer that experiences the behavior depicted in Fig. 2.

Additionally, it is known that (Ampere's law), for a layer with *N* turns and breadth b_w

$$H(h,0) - H(0,0) = \frac{N \cdot i_1}{b_w} \| H(h,t_f) - H(0,t_f) = \frac{N \cdot i_2}{b_w}. \quad (9)$$

All these equations allow magnetic field evolution to be determined. The complete problem, including boundary conditions, is summarized in Fig. 7. Note that boundary conditions and initial and final situations are easily obtained from the low-frequency MMF diagrams.

These equations will be used in this section and in the following one to calculate magnetic field and current density evolutions after switching. While this is a topic of large interest for magnetic elements researchers, most SMPS designers may just be interested in knowing how to derive total losses as a function of the winding strategy used. Readers included in the latter group may skip these sections and refer to (28) at the end of Section IV.

The problem depicted in Fig. 7 will allow designers to derive the evolution of a magnetic field, by using an equation that

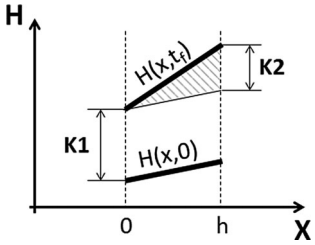

Fig. 8. Determination of *K*1 and *K*2.

responds to the following general type:

$$\frac{\partial^2 U(x,t)}{\partial x^2} = \frac{1}{\alpha^2} \cdot \frac{\partial U(x,t)}{\partial t}. \tag{10}$$

This is a classified differential equation known as "heat equation" whose solution can be found in several specialized books (such as [23], for instance) to be

$$U(x,t) = U_f\,(x) + \sum_{n=1}^{\infty} \left[b_n \cdot e^{-\frac{n^2 \cdot \pi^2 \cdot \alpha^2 \cdot t}{h^2}} \cdot \sin\left(\frac{n \cdot \pi \cdot x}{h}\right)\right] \tag{11}$$

where

$$b_n = \frac{2}{h} \cdot \int_0^h \left[U_i\,(x) - U_f\,(x)\right] \cdot \sin\left(\frac{n \cdot \pi \cdot x}{h}\right) dx \tag{12}$$

and $U_i(x)$ and $U_f(x)$ are, respectively, the initial and final distributions of *U*.

It is curious to see that the evolution of the magnetic field inside the winding equals that of the temperature distribution inside a material when two new temperatures are applied on both its lateral surfaces.

Replacing *U* by *H* in these expressions so that $U_i(x) = H(x,0)$ and $U_f(x) = H(x,t_f)$, and taking into account (7) and (8), parameters b_n can be calculated to be

$$b_n = \frac{2 \cdot K1}{n \cdot \pi} \cdot \left[1 - \cos\left(n \cdot \pi\right)\right] - \frac{2 \cdot K2}{n \cdot \pi} \cdot \cos\left(n \cdot \pi\right)$$
$$\text{with } K1 = \left[H\,(0,0) - H\,(0,t_f)\right]$$
$$K2 = \left[H\,(h,0) - H\,(h,t_f)\right] - \left[H\,(0,0) - H\,(0,t_f)\right]. \tag{13}$$

Note that the values of *K*1 and *K*2, however laborious their expressions might seem, can be very easily obtained from the MMF diagrams corresponding to instants $t = 0$ and $t = t_f$. Fig. 8 shows this.

Also, it is important to note that b_n does not depend on the value of the layer width, *h*, although this parameter appears in the definition of the problem: b_n just depends on the magnetic field changes that occur on the boundaries of the conductor layer.

The final solution to our problem yields

$$H(x,t) = H\,(x,t_f) + \sum_{n=1}^{\infty} \left[b_n \cdot e^{-\frac{n^2 \cdot \pi^2}{h^2 \cdot \mu \cdot \sigma'} \cdot t} \cdot \sin\left(\frac{n \cdot \pi \cdot x}{h}\right)\right]. \tag{14}$$

TABLE I
SLOWEST DIFFUSIVITY TIMES FOR DIFFERENT LAYER WIDTHS ($\eta \approx 1$)

h [mm]	τ_1 [μs]
0.1	0.07
0.2	0.29
0.5	1.81
1.0	7.26

From this result, it is possible to say that the value of magnetic field, *H*, consists of the steady-state value, $H(x,t_f)$, plus several waveforms in the form of exponential evolutions decreasing at different rates (with different time constants). These rates, $_n$, (which will be referred to as diffusivity for similarity with the equivalent thermal problem), depend on the material used for the layer (μ, σ') and on its thickness (*h*)

$$\tau_n = \frac{h^2 \cdot \mu \cdot \sigma'}{n^2 \cdot \pi^2}. \tag{15}$$

The slowest of these exponential waveforms corresponds to $n = 1$. Table I shows the values of $_1$ associated with different layer widths, *h*. The information included in this table assumes the windings are foil conductors with a layer porosity factor close to unity. For other type of windings, it must be taken into account that the lower the porosity factor, the lower the value of $_1$. As expected, it can be said in general terms that the thicker the layer, the longer the diffusivity time, which means that the switching—or rather the nonuniform field and current distribution—takes longer in thicker wires to be completed.

IV. SWITCHING LOSS CALCULATION

Now, we have obtained the evolution of the magnetic field within a layer during current switching; we can use this to determine the losses produced in the process. Equation (2) can be more precisely rewritten as follows:

$$\frac{\partial H_Z}{\partial x} = -J_Y\,. \tag{16}$$

And, substituting (14) into this expression yields

$$J_Y\,(x,t) = -\left[\frac{H\,(h,t_f) - H\,(0,t_f)}{h} + \sum_{n=1}^{\infty} \left[b_n \cdot e^{-\frac{n^2 \cdot \pi^2}{h^2 \cdot \mu \cdot \sigma'} \cdot t} \cdot \frac{n \cdot \pi}{h} \cdot \cos\left(\frac{n \cdot \pi \cdot x}{h}\right)\right]\right] \tag{17}$$

which, according to (9), can also be rewritten as

$$J_Y\,(x,t) = -\left[\frac{N \cdot i_2}{b_w \cdot h} + \sum_{n=1}^{\infty} \left[b_n \cdot e^{-\frac{n^2 \cdot \pi^2}{h^2 \cdot \mu \cdot \sigma'} \cdot t} \cdot \frac{n \cdot \pi}{h} \cdot \cos\left(\frac{n \cdot \pi \cdot x}{h}\right)\right]\right] \tag{18}$$

where the first term in the square brackets represents the steady-state current density, J_f, once the switching has been completed

$$J_f = \frac{N \cdot i_2}{b_w \cdot h}. \tag{19}$$

Now, we can use this expression to obtain the total losses in the winding at a given instant *t*, which can be calculated as

$$P(t) = b_w \cdot \mathit{length} \cdot \int_0^h \frac{J_Y^2(x,t)}{\sigma'} dx \tag{20}$$

where *length* is the total average length of the layer considered. By squaring the expression in (18) and adequately substituting that value into (20), the following result is obtained:

$$\begin{aligned} P(t) &= b_w \cdot \mathit{length} \cdot h \cdot \frac{J_f^2}{\sigma'} + \left[\frac{b_w \cdot \mathit{length} \cdot h}{2 \cdot \sigma'} \right. \\ &\quad \left. \cdot \sum_{n=1}^{\infty} \left[b_n^2 \cdot e^{-2 \cdot \frac{n^2 \cdot \pi^2}{h^2 \cdot \mu \cdot \sigma'} \cdot t} \cdot \left(\frac{n \cdot \pi}{h}\right)^2 \right] \right] \\ &= P_{\mathrm{DC}} + P_{\mathrm{switch}}(t). \end{aligned} \tag{21}$$

Although this equation already accounts for the instantaneous value of the power lost in the winding, designers might be interested in having a simpler expression that allows them to easily determine the total losses associated with different wire thicknesses.

From (21), it is possible to obtain the energy lost within the period that takes place after the current has switched from i_1 to i_2. In what follows, that period will be assumed to be the on-period, T_{on}. The same could be applied to T_{off}

$$\begin{aligned} E_{\mathrm{on}} &= \int_0^{T_{\mathrm{on}}} P(t) dt \\ &= b_w \cdot \mathit{length} \cdot h \cdot \frac{J_f^2}{\sigma'} \cdot T_{\mathrm{on}} + \frac{b_w \cdot \mathit{length} \cdot h}{2 \cdot \sigma'} \\ &\quad \cdot \sum_{n=1}^{\infty} \left[b_n^2 \cdot \left(\frac{n \cdot \pi}{h}\right)^2 \cdot \int_0^{T_{\mathrm{on}}} e^{-2 \cdot \frac{t}{\tau_n}} dt \right] \\ \text{with } \tau_n &= \frac{h^2 \cdot \mu \cdot \sigma'}{n^2 \cdot \pi^2}. \end{aligned} \tag{22}$$

Solving the integral in (22) yields

$$\begin{aligned} E_{\mathrm{on}} &= \frac{b_w \cdot \mathit{length} \cdot h}{\sigma'} \cdot J_f^2 \cdot T_{\mathrm{on}} + \frac{b_w \cdot \mathit{length} \cdot h}{4} \\ &\quad \cdot \sum_{n=1}^{\infty} \left[b_n^2 \cdot \mu \cdot \left(1 - e^{-2 \cdot \frac{T_{\mathrm{on}}}{\tau_n}}\right) \right]. \end{aligned} \tag{23}$$

The first part of this expression is the dc energy, whereas the second term accounts for the switching energy (switching copper losses). If enough time is allowed, the instantaneous switching energy loss will become null and a steady-state operation will be defined. The method described in this paper assumes that the switching is fully completed, which would result in $e^{-2 \cdot T_{\mathrm{on}}/\tau_n} \approx 0$. In order for this to be so, it must be guaranteed that the T_{on} period is greater than the time t_f that takes the exponential evolution to be completed. Theoretically, this time would be infinite, but it is usually accurate enough, for designing purposes, to assume the exponential evolution is complete when switching loss falls below 5% its initial value, which results in $t_f \approx 1.5 \cdot \tau_n$. Table II shows the minimum T_{on} values required to use the method described in this paper. These values have been calculated considering τ_1, which is the longest of all the diffusivity times.

TABLE II
SWITCHING TIME REQUIRED

h [mm]	t_f [μs]
0.1	0.11
0.2	0.44
0.5	2.72
1.0	10.89

According to this, as long as T_{on} (and T_{off}) in the current waveform is at least as long as the times indicated in Table II (for the selected windings), the switching can be considered to be complete, and therefore

$$E_{\mathrm{on}} = P_{\mathrm{dc}} \cdot T_{\mathrm{on}} + \frac{b_w \cdot \mathit{length} \cdot h}{4} \cdot \mu \cdot \sum_{n=1}^{\infty} b_n^2. \tag{24}$$

According to this expression, the energy lost during T_{on} originated by the switching can be calculated as the summation of series defined by parameters b_n squared. This can be done by taking into account the definition of these parameters provided by (13) together with the information included in Fig. 7 and applying certain trigonometry and harmonic series definitions, such as

$$\begin{aligned} &\cos(n \cdot \pi) = (-1)^n, \quad \cos^2(n \cdot \pi) = 1 \\ &\sum_{n=1}^{\infty} \frac{(-1)^n}{n^2} = -\frac{1}{12} \cdot \pi^2, \quad \sum_{n=1}^{\infty} \frac{1}{n^2} = \frac{1}{6} \cdot \pi^2. \end{aligned} \tag{25}$$

The result thus obtained is

$$\sum_{n=1}^{\infty} b_n^2 = 2 \cdot \left(K1^2 + K1 \cdot K2 + \frac{1}{3} \cdot K2^2 \right) \tag{26}$$

which yields

$$\begin{aligned} E_{\mathrm{on}} &= P_{\mathrm{DC}} \cdot T_{\mathrm{on}} + \frac{b_w \cdot \mathit{length} \cdot h}{2} \cdot \mu \\ &\quad \cdot \left(K1^2 + K1 \cdot K2 + \frac{1}{3} \cdot K2^2 \right). \end{aligned} \tag{27}$$

It must be noted that parameters *K*1 and *K*2 included in this expression were defined in (13) as a function of the difference $H(x,0)$–$H(x,t_f)$, where either $x = 0$ or $x = h$. This means that energy lost during the switching is only dependent on the value of the magnetic field before and after the switching has taken place, not on the transient evolution of such field. This value can be graphically represented as shown in Fig. 9.

Note from Fig. 9(b) that copper switching copper energy losses are equal to the magnetic energy variations inside the conductor (if no initial or final magnetic field in the winding).

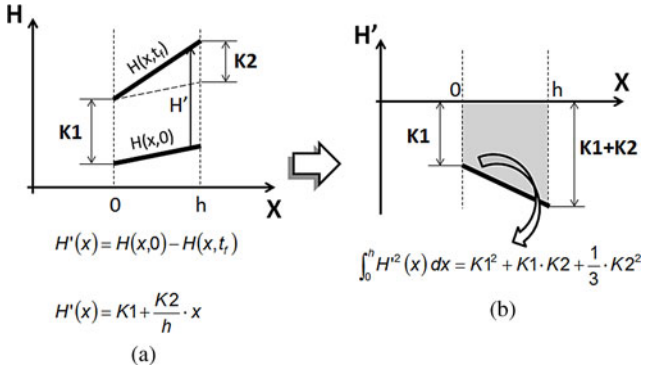

Fig. 9. (a) Initial and final magnetic field distribution in a winding. (b) Magnetic-field variation and contribution to the energy lost during switching.

It can thus be concluded that the energy lost in an N-turn layer of width h that conducts an RMS current i_2 during the on-time equals

$$E_{\rm on} = \frac{1}{\sigma'} \cdot \frac{\mathit{length}}{b_w \cdot h} \cdot N^2 \cdot i_2^2 \cdot T_{\rm on} + \frac{b_w \cdot \mathit{length} \cdot h}{2} \cdot \mu \cdot \left(K1^2 + K1 \cdot K2 + \frac{1}{3} \cdot K2^2 \right). \quad (28)$$

This energy can be divided into two different terms: the dc energy, obtained using the traditional expression, plus the switching energy, that has been demonstrated to be dependent only on the initial and final magnetic field distributions in the layer considered. This expression contributes to making it easier for designers to optimize the magnetic component they are developing, for they can have some insight into the copper losses the device gives rise to depending on the dimensions and disposition of the windings used. Not only can they observe the influence of geometrical parameters (such as b_w, *length* or h), but also the influence of winding strategy, since parameters $K1$ and $K2$ account for the influence neighboring conductors can have on a given layer. Designers can redistribute layers in order to minimize the influence of this factor.

It can also be observed that increasing layer thickness, h, will reduce the first part of the energy loss expression (the dc term), whereas losses produced due to magnetic field change (copper switching losses) will increase. This indicates the existence of an optimal value of the layer thickness for each application.

V. Analysis Example

Once the final expression has been derived, designers do not need to use all the equations that have been required to obtain it. All they have to do is apply (28) and determine whether the winding strategy used for their transformer would give rise to acceptable losses or not. In order to demonstrate how easily this could be achieved, a practical example is provided below.

Assume a 50-KHz 2:1 center-tap secondary bridge transformer is to be developed. For the sake of convenience, we will consider its winding pattern that is represented in Fig. 4 together with the current flowing through the windings. The converter chosen is a 40–10-V, 60-W half-bridge, and the core to use is of the type RM10. We will consider a primary peak current of 3 A, which results in 6-A peak current flowing through the secondary windings.

The primary side is made up using a 0.5-mm-thick wire and consists of 40 turns split into two 20-turn layers. The secondary consists of two 20-turn windings A and B, made up using a 1-mm-thick wire, each of them formed by two layers. The average turn length is 50 mm.

Determination of the copper loss in the structure depicted in Fig. 4 is achieved by using a simple spreadsheet like that shown in Fig. 10. This spreadsheet, or a similar one, can be easily obtained by following steps 1–4 indicated below.

Step 1 (Low-frequency MMF diagrams): Rows 1–4 include the $N{\cdot}I$ values corresponding to each of the six layers in the transformer, for the four converter stages. From these values, the MMF diagrams (rows 5–8) are easily obtained by adding the $N{\cdot}I$ values starting from the right [Ampere's law, Fig. 4(c)].

Step 2 (DC losses): The $N{\cdot}I$ values can also be used to derive dc copper losses in the transformer windings. Rows 9–12 show the dc copper losses at each stage. In order to clearly show the influence of each stage on the total losses, these dc power losses have been averaged to a complete switching period using the following equation:

$$\text{Losses}_{\rm DC} = \frac{1}{\sigma} \cdot \frac{\mathit{length}}{\pi/4 \cdot d^2 \cdot N} \cdot (N \cdot i_2)^2 \cdot \frac{T_{\rm stage}}{T} \quad (29)$$

where T is the switching period (1/frequency) and d is the wire diameter of the winding considered.

Step 3 (Constants K1 and K2): $K1$ and $K2$ are related to magnetic field variations from one stage to the next. The values of the magnetic field are obtained by dividing the MMF values over the core breadth. However, for the sake of clarity, rows 16–23 use only MMF values to calculate these constants for all the transitions from one stage to the next (these values will be later divided by the core breadth in order to derive the actual value of switching losses).

$K1$ is calculated as the MMF variation at the left of a layer, the values of which had been included in rows 5–8. As far as $K2$ is concerned, Fig. 8 shows that it can be calculated as the difference between the $K1$ value of that layer and the $K1$ value of the next layer at the right.

This information is already helpful, since higher $K1$ and $K2$ values (for a given conductor size) will produce higher copper switching losses. Thus, it can help designer to determine which layers should be relocated in order to reduce the values of these constants and, hence, high-frequency losses.

Step 4 (Calculation of switching energy and copper losses): Once constants $K1$ and $K2$ have been determined, the switching losses associated with each stage transition can be derived. Rows 25–28 include these switching losses, calculated for round wire using (30); the values of constants $K1$ and $K2$ included in the spreadsheet have been divided by the core breadth b_w before

	Layer	A1	A2	B1	B2	P2	P1	
1	1-NI	-60	-60	0	0	60	60	
2	2-NI	-30	-30	30	30	0	0	
3	3-NI	0	0	60	60	-60	-60	
4	4-NI	-30	-30	30	30	0	0	
5	1-MMF(LEFT)	0	60	120	120	120	60	0
6	2-MMF(LEFT)	0	30	60	30	0	0	0
7	3-MMF(LEFT)	0	0	0	-60	-120	-60	0
8	4-MMF(LEFT)	0	30	60	30	0	0	0
9	1-DC	0,099	0,099	0,000	0,000	0,198	0,198	
10	2-DC	0,025	0,025	0,025	0,025	0,000	0,000	
11	3-DC	0,000	0,000	0,099	0,099	0,198	0,198	
12	4-DC	0,025	0,025	0,025	0,025	0,000	0,000	TOTAL DC
13	TOTAL DC	0,148	0,148	0,148	0,148	0,395	0,395	1,383
14	TOTAL DC winding		0,296		0,296		0,790	
15								
16	K1 1-SW (TO=4, TF=1)	0,000	30,000	60,000	90,000	120,000	60,000	0
17	K1 2-SW (TO=1, TF=2)	0,000	-30,000	-60,000	-90,000	-120,000	-60,000	0
18	K1 3-SW (TO=2, TF=3)	0,000	-30,000	-60,000	-90,000	-120,000	-60,000	0
19	K1 4-SW (TO=3, TF=4)	0,000	30,000	60,000	90,000	120,000	60,000	0
20	K2 1-SW (TO=4, TF=1)	30,000	30,000	30,000	30,000	-60,000	-60,000	
21	K2 2-SW (TO=1, TF=2)	-30,000	-30,000	-30,000	-30,000	60,000	60,000	
22	K2 3-SW (TO=2, TF=3)	-30,000	-30,000	-30,000	-30,000	60,000	60,000	
23	K2 4-SW (TO=3, TF=4)	30,000	30,000	30,000	30,000	-60,000	-60,000	
24								
25	1-SW (TO=4, TF=1)	0,035	0,244	0,661	1,287	0,487	0,070	
26	2-SW (TO=1, TF=2)	0,035	0,244	0,661	1,287	0,487	0,070	
27	3-SW (TO=2, TF=3)	0,035	0,244	0,661	1,287	0,487	0,070	
28	4-SW (TO=3, TF=4)	0,035	0,244	0,661	1,287	0,487	0,070	TOTAL SW
29	TOTAL SW	0,139	0,974	2,644	5,149	1,948	0,278	11,134
30	TOTAL SW winding		1,113		7,794		2,227	
31	TOTAL WINDING		1,410		8,090		3,017	
32								
33	TOTAL LOSSES			12,517				

Fig. 10. Example of spreadsheet used to calculate transformer copper losses.

using them in the equation

$$\text{Losses}_{\text{switching}} = \frac{b_w \cdot \mathit{length} \cdot \sqrt{\pi/4} \cdot d}{2 \cdot T} \cdot \mu \cdot \left(K1^2 + K1 \cdot K2 + \frac{1}{3} \cdot K2^2 \right). \quad (30)$$

These switching losses have also been averaged to one switching period, just as had been done with the dc losses.

Some cells have also been added in the spreadsheet including losses for each winding: dc, switching, and total.

Other interesting information that can be obtained from this spreadsheet is related to the optimum conductor size to be used in the winding. Equations (29) and (30) show that total winding losses can be expressed as follows:

$$\text{Losses}_{\text{Total}} = \text{Losses}_{\text{dc}} + \text{Losses}_{\text{switching}} = \frac{C1}{d^2} + C2 \cdot d \quad (31)$$

with $\text{Losses}_{\text{dc}}$ and $\text{Losses}_{\text{switching}}$ being the values included in rows 14 and 30, respectively. From this expression, the optimum wire diameter for the given layer disposition can be easily obtained as

$$d_{\text{Optimum}} = \sqrt[3]{\frac{2 \cdot C1}{C2}}. \quad (32)$$

For the transformer considered, optimum diameters for windings A, B, and P would be 0.81, 0.46, and 0.44 mm, respectively (using these diameters, it would be advisable to consider the possibility of using only one layer for winding B).

VI. Verification of the Expressions Derived

Experimental validation of the method presented is not an easy task. First, it is not possible to measure field and current density distributions inside the conductors. Additionally, currents in real converters are not going to be perfectly square, and other effects such as core losses or leakage inductance

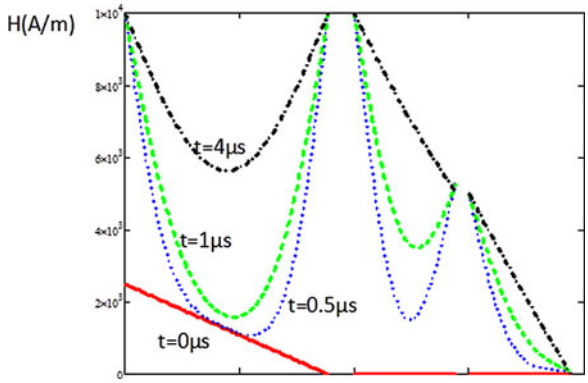

Fig. 11. Magnetic field distribution inside the layers during stage 1.

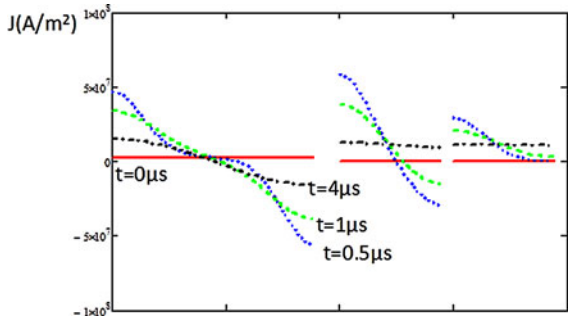

Fig. 12. Current density distribution inside the layers during stage 1.

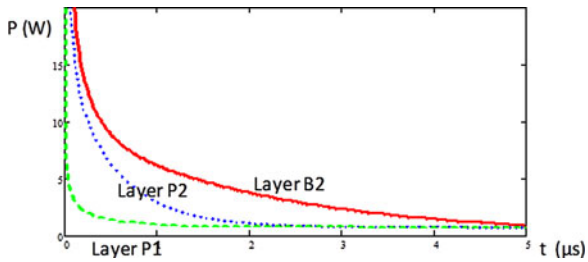

Fig. 13. Power losses in the layers during stage 1.

resonance (which very much depend on the layer arrangement) will also affect the transformer behavior. This is why all the previous works referenced in this paper verify the models developed by comparing their results with those provided by mathematical resolution (usually Fourier analysis).

Due to these reasons, verification of the results yielded by the method described in this paper is carried out following three different comparison criteria.

1) As far as the mathematical development from Maxwell's equations is concerned, the results provided by the equations derived in this paper related to magnetic field, current density distribution, and power losses versus time will be verified against a mathematical software solver.
2) Since the method presented in this study is meant to determine transformer copper losses for squared-current waveforms, it must be compared with previous methods that are not limited to sinusoidal waveforms. The work developed by Vandelac and Ziogas [22] has been chosen for this purpose.
3) Finally, several transformer designs, with different wire sizes and layers arrangements, have been tested on a real converter in order to verify global efficiency variations.

For the first step in the verification process, a mathematical software (Mathcad) has been used to solve the problem set out in Fig. 7 (applied to the case depicted in Section V) in order to compare the results obtained and those provided with the proposed method.

As was to be expected, equations (10)–(21) perfectly match the results provided by the mathematical software, since these equations are simply the result of using the well-known solution of the so-called heat equation in the time domain. All the same, this result proves that no error has been made when applying the heat equation to the electromagnetic problem depicted in Fig. 7.

Fig. 11 shows different instants of the magnetic field evolution inside the three outmost layers of transformer shown in Fig. 4, with the values indicated in Section V. It can be seen that primary layers reach the final magnetic field faster than the winding B layer (this is so because higher thickness involves lower diffusivity).

Similarly, the current density inside the same three layers is represented in Fig. 12. This figure is good evidence of the high-frequency effects in SMPS. The current through the layer at the right must change from 0 to 6 A. Since the magnetic field cannot change instantaneously, current flows only at the conductor sides at the beginning, and it takes some time (which is a function of the material electromagnetic properties and its dimensions) for that current to become uniformly distributed (skin effect in the time domain).

Moreover, the layer at the left is supposed to conduct no current during this stage. However, due to the variations of the magnetic field created on it by the other layers, large currents are induced inside this layer, giving rise to copper losses even though the total layer current is zero (proximity effect).

Current density information allows total layer losses to be plotted as a function of time. Fig. 13 shows the instantaneous power loss during this stage.

Table III compares the losses at stage 1 obtained with the mathematical software and those obtained using the method proposed in this paper (spreadsheet in Fig. 10). The small discrepancy in layer B2 is produced because (28) computes losses considering the magnetic field has fully changed, whereas the magnetic field inside layer B2 (1 mm thick, which has an associated skin depth of 0.295 mm) does not reach the final magnetic field distribution in the 5 μs that lasts stage 1 (see Figs. 11–13).

TABLE III
POWER LOSSES (W) AT STAGE 1 (AVERAGED TO ONE COMPLETE T)

	Mathematical solver	Proposed method *(DC+SW)*
Layer B2	1.186	1.287 (0 + 1.287)
Layer P2	0.684	0.685 (0.198 + 0.487)
Layer P1	0.267	0.268 (0.198 + 0.070)

TABLE IV
THEORETICAL/MEASURED POWER LOSSES (W)

		T1	T2	T3	T4
Theoretical losses	Total	5.21	4.13	4.93	1.04
	DC	0.76	1.46	2.46	0.76
	Switching	4.45	2.67	2.47	0.28
Theoretical loss difference with respect to T2		+1.08	0	+0.80	−3.89
Experimental loss variation with respect to T2		+1.4	0	+0.2	−4.4

As indicated above, a second level of verification consisted in comparing the results yielded by the method proposed to those produced by the work developed by Vandelac and Ziogas [22]. Considering the innermost winding, W_A, and the outmost one, W_P, the total losses provided by the method described in this paper are 1.41 and 3.017 W, respectively, whereas [22, eq. (42)] results in total losses of 1.28 W for W_A and 2.85 W for W_P. At this point, it must be said that, while the method proposed has used the simple operations included in the spreadsheet in Fig. 10, the results calculated as indicated in [22] has required calculating Fourier series and adding the first 100 harmonics.

For the case of winding W_B, it is not possible to compare our results with those of other references, since all previous works consider that the magnetic field at the winding sides depends on the current through that winding only.

Finally, four transformer designs have been tested on the converter described at the beginning of Section V. All the four transformers have a 40-turn primary winding, P, split into two layers (P1 and P2), and two 20-turn secondary windings, A and B, also split into two layers each (A1, A2, B1, and B2). In all the cases, an RM10 core is used.

Transformers T1, T2, and T3 use the layer arrangement shown in Fig. 4 and considered in Fig. 10: A1, A2, B1, B2, P2, and P1. Wire diameters in these transformers are

1) T1: P winding: 0.45 mm
   A winding: 0.90 mm. B winding: 0.90 mm.
2) T2: P winding: 0.45 mm
   A winding: 0.80 mm. B winding: 0.40 mm (optimum values).
3) T3: P winding: 0.45 mm
   A winding: 0.25 mm. B winding: 0.25 mm.

Transformer T4 uses the same wire diameter as T1, only the layer arrangement is different; in this case, primary and secondary layers are interleaved: A1, P1, B1, A2, P2, B2.

In the tests performed, primary peak current was reduced to 2 A, thus resulting in a 40-W converter. This has been so because power losses in some of the transformers were too large when trying to transfer 60 W (as considered in Section V): excessive heating was produced in transformers T1, T2, and T3

It must be taken into account that it is not possible to measure only copper losses in a transformer operating with real SMPS waveforms—in fact, none of the main references of this paper does it. Short-circuit resistance measured for ac waveforms does not reflect the losses induced by actual proximity effect in the SMPS. Measuring input and output transformer voltages and currents and performing power computation offers poor results, mainly due to current probes and sampling limitations. To our knowledge, the best way to compare transformer performance is measuring average currents and voltages (dc) at the converter input and output, and comparing losses differences for the four transformers under test. Transformer T2 will be used as reference, and converter losses variations will be compared with theoretical copper losses variations.

Considering transformers T1, T2, and T3 (the ones with the same layer arrangement), experimental data confirm that the diameters used in T2 are close to the optimum values, since it is this transformer that gives rise to lower losses. It must be pointed out that changing wire diameters does not only affect winding resistance, it also has an influence on leakage inductance values (they reduce as diameters are reduced), and it is not possible to experimentally separate both effects when analyzing converter performance.

This is especially shown by T4 results, in which loss reduction is even higher than theoretical prediction because the model proposed does not include leakage inductance influence. All experimented designers already know, however, that interleaved transformers always improve converter performance.

This is a key point in the transformer design. Even more important than determining the value of the optimum diameters is choosing the optimum layer arrangement. With the method proposed in this paper, that task is easily done by just changing the first four rows in the spreadsheet shown in Fig. 10 and checking the losses each arrangement gives rise to. Once the best layer disposition is found, designers can easily obtain optimum diameters by using (31) and (32). Using other methods would involve repeatedly calculating a large number of Fourier transforms.

VII. CONCLUSION

A mathematical expression has been derived that allows switching losses in a transformer to be easily obtained. In order to do so, only low-frequency MMF diagrams (both, before, and after the switching) are required. The method can be applied to any switching-mode transformer without the restrictions used by previous works, which consider that the magnetic field at the winding sides depends on the current through that winding current only.

All the mathematical operations required for obtaining the final expression have been checked by means of a calculation software, Mathcad, in this case.

An analysis example has been included that shows how designers can use the expression derived without the need to use all the mathematical work behind. A simple spreadsheet allows both dc losses and switching losses to be computed. Results have been compared, when possible, with previous works, and experimental tests have been conducted using four different transformers that validate the method proposed.

This expression makes it easier to optimize transformer windings, since it provides quick information about how the different winding patterns will affect final copper losses. Designers can organize layer distribution in the component so that parameters $K1$ and $K2$, which somehow define the layer position as related

to the other windings, are optimized. Also, they can use the expression derived to determine the optimum layer width.

REFERENCES

[1] I. Lope, C. Carretero, J. Acero, R. Alonso, and J. M. Burdio, "AC power losses model for planar windings with rectangular cross-sectional conductors," *IEEE Trans. Power Electron.*, vol. 29, no. 1, pp. 23–28, Jan. 2014.

[2] K. J. Hartnett, J. G. Hayes, M. G. Egan, and M. S. Rylko, "CCTT-core split-winding integrated magnetic for high-power DC–DC converters," *IEEE Trans. Power Electron.*, vol. 28, no. 11, pp. 4970–4984, Nov. 2013.

[3] M. Urling, V. A. Niemela, G. R. Skuttt, and T. G. Wilson, "Characterizing high-frequency effects in transformer windings—A guide to several significant articles," in *Proc. IEEE Appl. Power Electron. Conf.*, 1989, pp. 373–385.

[4] P. L. Dowell, "Effects of eddy currents in transformer windings," *Proc. IEE*, vol. 113, no. 8, pp. 1387–1394, Aug. 1966.

[5] M. P. Perry, "Multiple layer series connected winding design for minimum losses," *IEEE Trans. Power App. Syst.*, vol. PAS-98, no. 1, pp. 116–123, Jan./Feb. 1979.

[6] J. Rosa, "Calculation of flux linkages in multiwinding transformers," in *Proc. IEEE Power Electron. Spec. Conf.*, 1986, pp. 639–644.

[7] N. R. Coonrod, "Transformer computer design aid for higher frequency switching power supplies," in *Proc. IEEE Power Electron. Spec. Conf.*, 1984, pp. 257–267.

[8] P. S. Venkatraman, "Winding eddy current losses in switch mode power transformers due to rectangular wave currents," in *Proc. Powercon 11*, Ventura, CA, USA, 1984, pp. 1–11.

[9] B. Carsten, "High frequency conductor losses in switchmode magnetics," in *Proc. High-Freq. Power Converter Conf.*, 1986, pp. 155–176.

[10] J. Jongsma, "Minimum-loss transformer windings for ultrasonic frequencies—Part 1: Background and theory," *Philips Electron. Appl. Bull.*, vol. 35, no. 3, pp. 146–163, 1978.

[11] J. Jongsma, "High-frequency ferrite power transformer and choke design—Part 3: Transformer winding design," *Philips Electronic Components and Materials Technical Publication*, no. 207, 1986.

[12] J. Jongsma, "Minimum-loss transformer windings for ultrasonic frequencies—Part 2: Design methods and aids," *Philips Electron. Appl. Bull.*, vol. 35, no. 4, pp. 211–226, 1978.

[13] W. G. Hurley, E. Gath, and J. G. Breslin, "Optimizing the AC resistance of multilayer transformer windings with arbitrary current waveforms," *IEEE Trans. Power Electron.*, vol. 15, no. 2, pp. 369–376, Mar. 2000.

[14] R. P. Wojda and M. K. Kazimierczuk, "Analytical winding size optimisation for different conductor shapes using Ampère's law," *IET Power Electron.*, vol. 6, no. 6, pp. 1058–1068, Jul. 2013.

[15] M. A. M. Cheema, J. E. Fletcher, D. Dorrell, and M. Junaid, "A novel approach to investigate the quantitative impact of harmonic currents on winding losses and short circuit forces in a furnace transformer," *IEEE Trans. Magn.*, vol. 49, no. 5, pp. 2025–2028, May 2013.

[16] D. Murthy-Bellur, N. Kondrath, and M. K. Kazimierczuk, "Transformer winding loss caused by skin and proximity effects including harmonics in pulse-width modulated DC–DC flyback converters for the continuous conduction mode," *IET Power Electron.*, vol. 4, no. 4, pp. 363–373, Apr. 2011.

[17] W. Frelin, L. Berthet, M. Petit, and J. C. Vannier, "Transformer winding losses evaluation when supplying non linear load," in *Proc. 44th Univ. Power Eng. Conf.*, 2009, pp. 1–5.

[18] J. A. Ferreira, "Improved analytical modeling of conductive losses in magnetic components," *IEEE Trans. Power Electron.*, vol. 9, no. 1, pp. 127–131, Jan. 1994.

[19] X. Nan and C. R. Sullivan, "An improved calculation of proximity-effect loss in high-frequency windings of round conductors," in *Proc. Power Electron. Spec. Conf.*, 2003, vol. 2, pp. 853–860.

[20] C. A. Baguley and B. Carsten, "The effect of DC bias conditions on ferrite core losses," *IEEE Trans. Magn.*, vol. 44, no. 2, pp. 246–252, Feb. 2008.

[21] C. E. Hawkes, T. G. Wilson, and R. C. Wong, "Magnetic-field-intensity and current-density distributions in transformer windings," in *Proc. IEEE Power Electron. Spec. Conf.*, 1989, pp. 1021–1030.

[22] J. P. Vandelac and P. Ziogas, "A novel approach for minimizing high frequency transformer copper losses," in *Proc. IEEE Power Electron. Spec. Conf.*, 1987, pp. 355–367.

[23] W. E. Boyce and R. C. Diprima, "Partial differential equations and Fourier series," in *Elementary Differential Equations and Boundary Value Problems*. New York, NY, USA: Wiley, 2001, pp. 614–617.

Juan Manuel Lopera (M'96) was born in Avilés, Spain, in 1966. He received the M.Sc. and Ph.D. degrees in electrical engineering from the University of Oviedo, Gijón, Spain, in 1990 and 1994, respectively.

He is an Associate Professor at the University of Oviedo. His research interests include metal industry applications, magnetic elements, wireless sensors, and energy harvesting.

Dr. Lopera is the Technical Committee Papers Review Chair of the IEEE-IAS Metals Committee.

Miguel Jose Prieto (M'97) was born in Gijón, Spain, in 1969. He received the M.Sc. and Ph.D. degrees from the University of Oviedo, Gijón, in 1994 and 2000, respectively.

He joined the University of Oviedo in 1995, where he is currently an Associate Professor, having been involved in several research projects. Although his main research interest deals with magnetic components (his work covers various aspects from magnetic integration for power converters to industrial sensors based on magnetism), he has also worked in other fields, such as switching-mode power supplies, piezoelectric transformers, and microcontroller-based systems.

Juan Díaz (M'02) received the M.Sc. and Ph.D. degrees in electrical engineering from the University of Oviedo, Gijón, Spain, in 1990 and 1995, respectively.

He joined the University of Oviedo in 1990, and since then, he has been participating in several research and development projects. His research interests include switching-mode power supplies, resonant power conversion, piezoelectric transformers, dc high-voltage applications, and design of systems based on microcontrollers.

Jorge García (S'01–M'05–SM'11) received the M.Sc. and Ph.D. degrees in electrical engineering from the University of Oviedo, Asturias, Spain, in 2000 and 2003, respectively.

In December 1999, he joined the Electrical and Electronic Engineering Department, University of Oviedo, where he is currently an Associate Professor. His research interests include power electronic converters (power topologies, control schemes, and modeling), digital control, integration of stages, magnetic components, lighting electronics, and industrial applications. He is the coauthor of more than 30 journal papers and more than 60 international conference papers in power and industrial electronics.